

Aramid-Nanofiber-Reinforced Transparent Nanocomposites

Ming Yang^{1,†}, Keqin Cao,^{2,§} Bongjun Yeom,¹ M.D. Thouless,^{2,3,*} Anthony Waas,^{2,4,‡} Ellen M. Arruda,^{2,5,6,*} and Nicholas A. Kotov^{1,3,5,7,*}

¹Department of Chemical Engineering, University of Michigan, Ann Arbor, MI 48109;

²Department of Mechanical Engineering, University of Michigan, Ann Arbor, MI 48109;

³Department of Material Science and Engineering, University of Michigan, Ann Arbor, MI 48109

⁴Department of Aerospace Engineering, University of Michigan, Ann Arbor, MI 48109;

⁵Department of Biomedical Engineering, University of Michigan, Ann Arbor, MI 48109;

⁶Macromolecular Science and Engineering, University of Michigan, Ann Arbor, MI 48109;

⁷Biointerfaces Institute, University of Michigan, Ann Arbor, MI 48109;

[†]Present address: Key Laboratory of Microsystems and Microstructures Manufacturing, Ministry of Education, Harbin Institute of Technology, Harbin 150080.

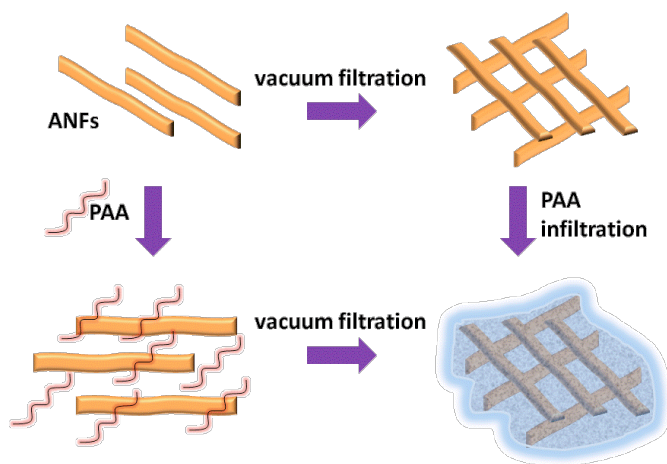
[§]Present address: Intel Corporation, 2501 NW 229th Ave, Hillsboro, OR 97124

[‡]Present address: Department of Aeronautics and Astronautics, University of Washington, Seattle, WA 98195-

E-mail: thouless@umich.edu, arruda@umich.edu; kotov@umich.edu

ABSTRACT: Nanoscale polymeric fibers are expected to bring about exceptional mechanical and optical properties in composite materials related to the better integration of different properties between fibers and polymers. The discovery of the first aramid nanofiber dispersion (*ACS Nano*. **2011**, *5*, 6945-6954) from commercial para-aramid macrofibers similar to Kevlar[®] developed by DuPont allowed the emergence of an innovative nanoscale building block with great potential for engineering novel high-performance polymer nanocomposites (*Adv. Funct. Mater.* **2013**, *23*, 2072-2080). Here we report the fabrication of aramid-nanofiber reinforced polyacrylic-acid thin films using vacuum-assisted flocculation. We show that the resulting composite has high transparency owing to the nanoscale size of the fibers. The multiple hydrogen bonds available at the interface between the polyacrylic acid and nanofibers result in significant improvement of mechanical properties, with Young's modulus outperforming single-walled carbon nanotube composites. The successful use of ANFs in producing transparent, strong, and flexible polymer nanocomposites indicates their great potential as an effective reinforcing agent in optical applications.

KEYWORDS: polymer nanofibers, aramid nanofibers, Kevlar[®], transparent nanocomposites, fiber-reinforced polymers, vacuum-assisted flocculation (VAF)



Fiber-reinforced polymers (FRPs)¹ integrate strong fibers (glass, carbon, and aramid fibers) and a polymer matrix into one entity to achieve a combination of desirable properties not available in any single conventional material. In particular, interface engineering through the modulation of the interfacial bonding strength allows load transfer to the fibers with high fidelity, resulting in composites with exceptional properties in terms of high stiffness and strength. In addition to their applications in the aerospace, automotive, marine, and construction industries, the significance of mechanical reinforcement of optically functional materials has been witnessed by the rapid growth of electronic industries which, in turn, have created a great demand for transparent, strong, and flexible materials.² However, traditional FRPs made with macroscale fibers generally yield opaque or non-transparent composites, which are not suitable for optical applications.

The availability of nanofibers with diameters significantly smaller than the wavelengths of visible light provide a possible way to circumvent this limitation of opaqueness. Avoiding the mismatch of refractive indices between the fiber and the matrix results in much less light scattering. For example, Nylon nanofibers with diameters 50-200 nm produced by electrospinning, were used to prepare an optically transparent composite with low-fiber volume content (3.9 %).³ Alternatively, high-fiber volume (70 %) transparent composites were obtained by using cellulose nanofibers with smaller diameters (15-20 nm).⁴ Despite the variety of potential sources of cellulose,⁵ their typical low aspect ratios could diminish the advantage of nanofibers for effective stress-transfer in composites and the lack of flexibility for conformational changes could be a problem for maximizing the interfacial attraction with nanoscale component of the composite.⁶ Furthermore, the hygroscopic nature of cellulose

nanofibers makes them very sensitive to humidity changes, reducing their mechanical performance under certain circumstances.⁷ It is therefore important to have processable synthetic polymer nanofibers with diameters comparable to or even smaller than cellulose nanofibers to achieve (1) higher volume reinforcement with good transparency as a result of the nanoscale effect; (2) effective stress-transfer from the fiber to polymer matrix based on the structural control and tunability of the intermolecular interactions of synthetic polymers; and (3) high environmental stability as a result of a highly crystalline structure.

Aramid macroscale fibers, most commonly known as Kevlar[®], are prepared by spinning a liquid concentration of sulfuric acid into a crystallized fiber. Aramid fibers are well-suited to high performance FRP applications, because they combine a high specific strength and modulus with a high thermal resistance and chemical inertness. Furthermore, they exhibit low electrical conductivity compared to metallic or carbon fibers, which makes them suitable for high-performance supporting materials, insulation layers in electronics and coatings for glass to make it shatter resistant. With these unique properties, utilization of aramid fibers in transparent FRPs would be very attractive, however they still face a challenge due to their macro- and/or micro-scale structures. Recently, we reported the production of aramid nanofibers (ANFs) based on the controlled dissolution of Kevlar[®] macrofibers in a solution of DMSO and KOH.⁸ As stable dispersions of nanofibers are virtually unknown for synthetic polymers, the invention of an ANF dispersion could lead to broad applications such as protective coatings, ultrastrong membranes, and polymer nanocomposites. Our latest efforts showed that the hydrolysis and cross-linking of ANFs with phosphoric acid and glutaraldehyde resulted in aramid materials with tailorable properties.⁹ In this work, to further our previous studies, we demonstrate the possibility of using ANFs in FRPs, leading to transparent, strong, and flexible membranes. We show that the

nanoscale structure of ANFs not only results in highly transparent FRPs consisting of high volume fractions of synthetic polymer fibers (up to 95%), but also allows the optimum bonding between the fiber and the matrix to achieve high stiffness resulting from the surface reactivity and high surface-to-volume ratio of ANFs.

We employed a vacuum-assisted flocculation (VAF) method that involves vacuum filtering a dilute suspension of ANFs with periodic additions over a porous nylon filtration membrane (Whatman, 0.1 μm pore size, 47 mm diameter) (Figure 1a). As the solvent falls through the filter pores, ANFs are trapped on the surface of the filter, forming an interconnected network (Figure 1b). Compared with other methods for fabricating films consisting of nanofiber networks, including drop casting,¹⁰ spin coating,¹¹ dip-casting,¹² Langmuir-Blodgett deposition,¹³ and LBL assembly,¹⁴ the high efficiency of film production and good film homogeneity and uniformity make VAF an ideal method for the rapid production of high quality ANF-based membranes. For our experiment, additions of polyacrylic acid (PAA) solution (1%, 250 kDa) (0.1-20 mL) into 30 mL ANF dispersion in DMSO (0.02%) formed a PAA/ANF suspension, which was then vacuum filtered (Figure 1a). The film was then washed in boiling water for 2.5 h to remove excess PAA. An infiltration method was also used to prepare composites with a higher volume fraction of PAA (Figure 1a). For this, 4 mL DI water was first added into a 30 mL ANF/DMSO dispersion, which was then vacuum-filtered to form a pure ANF membrane. Then 20 mL of PAA (1%) solution was used to impregnate the ANF membrane, assisted by vacuum. The films were then peeled from the nylon filter simply by using tweezers after drying or after brief exposure to 1% HCl solution at room temperature (to partially dissolve the nylon). Both pure ANF film and composite film showed fibrous structure (Figure 1b,c) and the free-standing ANF reinforced PAA membrane retained the transparency of the amorphous PAA matrix (Figure

1d). The sheet was as foldable as conventional paper; this was illustrated by shaping the membrane into a simple model of an airplane with entire integrity (Figure 1e), indicating the composite is a flexible plastic.

A large mismatch between the refractive indices of PAA and Kevlar[®] (PAA is 1.395, and Kevlar[®] is 2.0 parallel to the fiber axis, and 1.6 perpendicular to the axis) increases light scattering, resulting in opacity. The small ANF diameters, which are much smaller than the wavelengths of visible light, are believed to be responsible for the high transparency of the composite film. The potential of using PAA/ANF suspensions in transparent coatings was further demonstrated by simple solution casting, corroborated by UV-Vis spectroscopy. The increased light absorption after additional layers (up to 5) occurred mainly in the UV range, originating from the absorption of Kevlar[®] (less than 400 nm), and the transparency of the glass slide coated with 15 nm thick PAA/ANFs was nearly the same as the uncoated one (Figure 2d, insets).

The strong interactions between PAA and ANFs have been evidenced by different techniques. It was found that the range of diameters of ANFs in DMSO is 20–30 nm. Previous models by Sawyer suggested a hierarchical fibrillar microstructure of Kevlar[®]; fibers with the smallest microfibrils/layers ranging in size from 3 to 30 nm wide, and 2-5 nm thick.¹⁵ Interestingly, our ANFs have comparable dimensions to the lower ends of these ranges, implying that the microfibrils may be the fundamental building blocks for such synthetic fibers. The diameters decrease with the addition of PAA, ultimately reducing to 5–10 nm when the volume ratio of PAA (1%) solution to DMSO is 1:7.5 (Figure 2a-c). Some change of ANF nanofibers diameter can occur due to varying composition of the media. The reason for the change in fiber diameter is not very clear at this point. We suspect that the addition of PAA solution may result in the reduction of surface charges, inducing the shrinkage of nanofibers into denser structures;

however, this may need further investigation. Furthermore, the addition of PAA may restore the protonation of ANFs, which results in a transition of the dominant absorption peak from around 400 nm (associated with the absorption of poly(p-phenylene terephthalamide) anions) to around 330 nm (associated with the absorption of neutral poly(p-phenylene terephthalamide) (Figure 3a). Such a transition would be more sensitive to PAA addition than to water (Figure 3b), owing to the higher acidity of the -COOH functional groups in the PAA. As a result, the negative surface charges that help disperse ANFs in DMSO will be greatly reduced upon the addition of PAA. However, we found that the PAA/ANF dispersion is very stable when the addition of PAA is more than 1 mL. A plausible explanation for this is based on the covalent cross-linking between PAA and ANFs. To illustrate this, IR spectra were taken to further investigate the interactions between PAA and ANFs (Figure 3c). The solvent effect on the IR peak of PAA, which can be assigned to the -C=O vibration, was clearly seen when DMSO was added to 1% PAA aqueous solution (Figure 3c, 1-2). The shift from 1733.97 cm^{-1} to 1737.82 cm^{-1} is probably caused by the disruption of the hydrogen bonding between PAA by DMSO. The addition of KOH in DMSO to the PAA solution broadened the IR peak at 1737.82 cm^{-1} ; this is probably caused by the more dissociated PAA, which can potentially enhance the hydrogen bonding between PAA molecules (Figure 3c, 3), and is confirmed by the shift in spectral position of the peak at in $2500\text{-}3500\text{ cm}^{-1}$ window. A noticeable peak shift from 1737.82 cm^{-1} to 1729.48 cm^{-1} was observed when PAA was mixed with ANFs (Kevlar[®] in DMSO and KOH solution) (Figure 3c (5)). Such a shift towards the lower energy in the spectrum implied the formation of hydrogen bonding between ANFs and PAA (Figure 3c (6)). There are potentially two types of hydrogen bonding that may exist at the interface of ANFs and PAA: The first is between -C-OH (PAA) and -C=O (ANFs), and the second is between -C=O (PAA) and -N-H (ANFs) (Figure 3d). We did not observe the

obvious peak shift from ANFs upon the addition of PAA; this might be caused by the overwhelming presence of similar hydrogen bonding within the structure of ANFs (Figure 3c (4-5)), diminishing the peak shift from the surface hydrogen bonding. The effective interfacial interactions between PAA and ANFs, as confirmed by the IR spectra, take advantage of the dense active functional groups on ANFs with their increased surface-to-volume ratio over macroscale fibers.

The volume fractions of PAA in the composite films were estimated by calculating the weight difference between the pure ANF film and the PAA/ANF composites (density of PAA is 1.14 g/cm^3 and that of Kevlar[®] is 1.44 g/cm^3). Different volume fractions of PAA (5%, 9%, 18%, 20%, 24% and 25%) in the resultant composites were obtained. The mechanical properties of the PAA/ANF films were characterized by room-temperature uniaxial tensile testing at a strain rate of 0.005/s. The thicknesses of composite films used for tensile tests were typically in the range of 4-5 μm . Generally, PAA/ANF films have increased moduli compared with that of a pure ANF film (Figure 4). This implies that PAA can effectively cross-link nanofibers forming continuous networks owing to the interfacial hydrogen bonds, as illustrated in Figure 3d. With 5% PAA, the modulus of an ANF network is increased from 7 GPa to 9 GPa (Figure 4). It was improved to 13 GPa with 9% PAA, and reached the highest value (20 GPa) with 20% PAA. Further increase in the volume fraction of PAA in the composite resulted in a decrease of the modulus to 12 GPa. It is speculated that while lower amounts of PAA promote cross-linking of the ANF matrix to enhance the modulus, excess PAA aggregates to form low-modulus PAA regions in the composites. Significantly, the modulus of our 20% PAA film (20 GPa) outperforms not only cellulose nanofiber based composite films (13 GPa),⁴ but also the recently reported single-walled

carbon nanotube reinforced polymer nanocomposites (13 GPa², 15 GPa¹⁶), demonstrating the great potential of ANFs as excellent reinforcement agents.

The change of the ultimate strength with volume fraction of PAA was not as consistent as the change in modulus (Figure 4). This could be caused by the sensitivity of the strength to the presence of defects. We believe that the initial loss of surface charges upon the addition of PAA may result in the aggregation of ANFs, causing the inhomogeneous distribution of ANFs in the composites and therefore reducing the ultimate strength. The mechanical properties of the 20 mL PAA infiltrated film included a similar modulus but lower ultimate strength when compared with the film made by the addition of 20 mL PAA (Figure 4), illustrating a high sensitivity of the composite properties to the processing methods.

In summary, transparent, strong, and flexible ANF-reinforced polymer nanocomposites with different volume fractions of PAA were fabricated by a vacuum-assisted flocculation method. The nanoscale structures of ANFs render the composite films with high transparency and significant mechanical reinforcement. Given the convenience of liquid-state processability and unique chemical and physical properties of ANFs, combinations with other polymers may result in a series of novel high-performance transparent composite materials.

REFERENCES

1. Bledzki AK and Gassan J. Composites reinforced with cellulose based fibres. *Prog Polym Sci* 1999; 24: 221-274.
2. Zhu J, Shim BS, Di Prima M and Kotov NA. Transparent Conductors from Carbon Nanotubes LBL-Assembled with Polymer Dopant with pi-pi Electron Transfer. *J Am Chem Soc* 2011; 133: 7450-7460.
3. Bergshoeff MM and Vancso GJ. Transparent nanocomposites with ultrathin, electrospun nylon-4,6 fiber reinforcement. *Adv Mater* 1999; 11: 1362-1365.
4. Yano H, Sugiyama J, Nakagaito AN, et al. Optically transparent composites reinforced with networks of bacterial nanofibers. *Adv Mater* 2005; 17: 153-155.
5. Eichhorn SJ. Cellulose nanowhiskers: promising materials for advanced applications. *Soft Matter* 7: 303-315.
6. Podsiadlo P, Tang Z, Shim BS and Kotov NA. Counterintuitive effect of molecular strength and role of molecular rigidity on mechanical properties of layer-by-layer assembled nanocomposites. *Nano Lett* 2007; 7: 1224-1231.
7. Cranston ED, Eita M, Johansson E, et al. Determination of Young's Modulus for Nanofibrillated Cellulose Multilayer Thin Films Using Buckling Mechanics. *Biomacromolecules* 12: 961-969.
8. Yang M, Cao KQ, Sui L, et al. Dispersions of Aramid Nanofibers: A New Nanoscale Building Block. *ACS Nano* 2011; 5: 6945-6954.
9. Cao K, Siepermann CP, Yang M, et al. Reactive Aramid Nanostructures as High-Performance Polymeric Building Blocks for Advanced Composites. *Adv Funct Mater* 2012: 2072-2080.

10. Sreekumar TV, Liu T, Kumar S, Ericson LM, Hauge RH and Smalley RE. Single-wall carbon nanotube films. *Chem Mater* 2003; 15: 175-178.
11. Meitl MA, Zhou YX, Gaur A, et al. Solution casting and transfer printing single-walled carbon nanotube films. *Nano Lett* 2004; 4: 1643-1647.
12. Spotnitz ME, Ryan D and Stone HA. Dip coating for the alignment of carbon nanotubes on curved surfaces. *J Mater Chem* 2004; 14: 1299-1302.
13. Kim Y, Minami N, Zhu WH, Kazaoui S, Azumi R and Matsumoto M. Langmuir-Blodgett films of single-wall carbon nanotubes: Layer-by-layer deposition and in-plane orientation of tubes. *Japanese Journal of Applied Physics Part 1-Regular Papers Short Notes & Review Papers* 2003; 42: 7629-7634.
14. Mamedov AA, Kotov NA, Prato M, Guldi DM, Wicksted JP and Hirsch A. Molecular design of strong single-wall carbon nanotube/polyelectrolyte multilayer composites. *Nature Mater* 2002; 1: 190-194.
15. Sawyer LC, Chen RT, Jamieson MG, Musselman IH and Russell PE. Microfibrillar structures in liquid-crystalline polymers. *J Mater Sci Lett* 1992; 11: 69-72.
16. Shim BS, Zhu J, Jan E, et al. Multiparameter Structural Optimization of Single-Walled Carbon Nanotube Composites: Toward Record Strength, Stiffness, and Toughness. *ACS Nano* 2009; 3: 1711-1722.

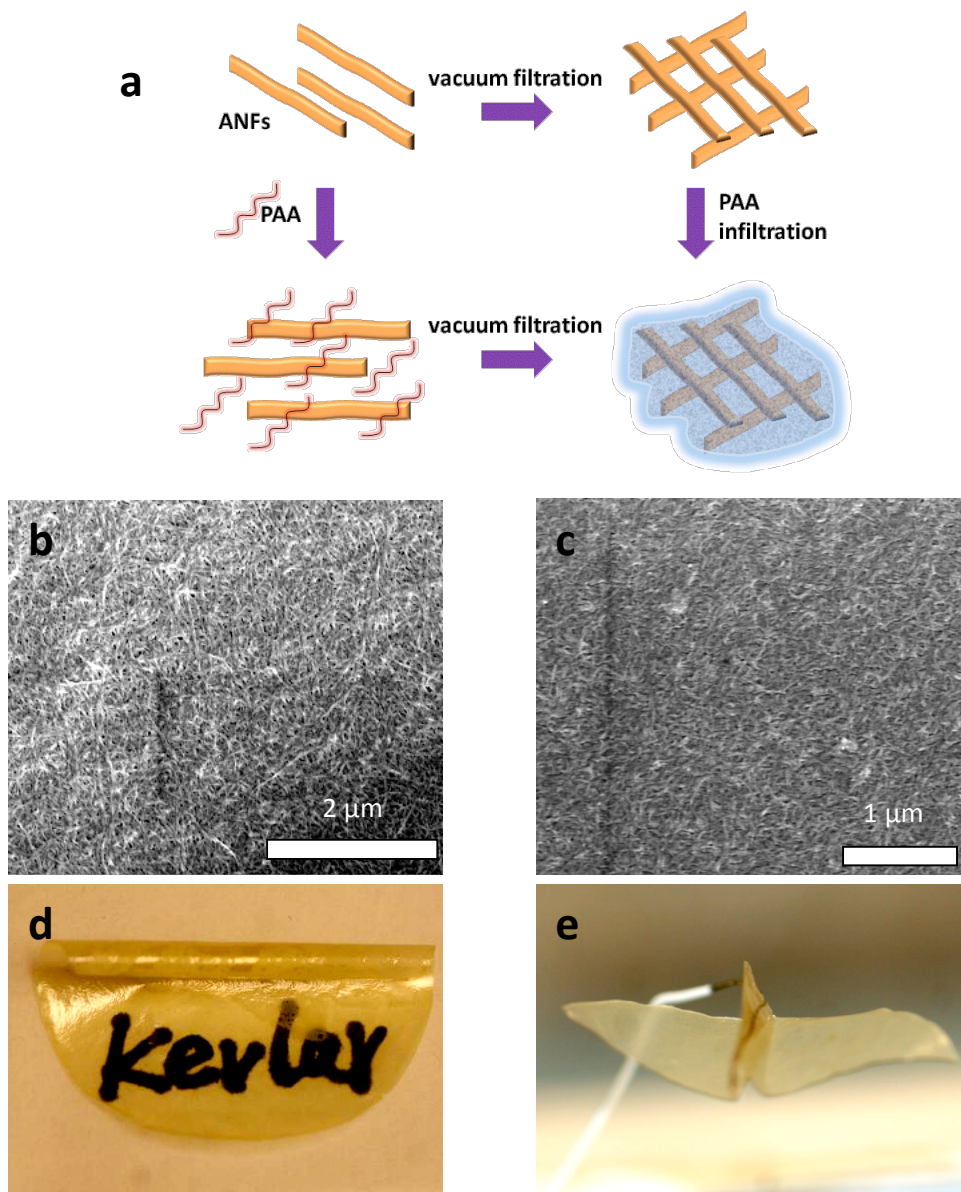


Figure 1. (a) Schematic illustration of the experimental design. SEM images of (b) pure ANF film and (c) PAA/ANF composite film obtained with the addition of 3 mL PAA. Optical images of composite films obtained with the addition of 3 mL PAA showing (d) transparency and (e) flexibility.

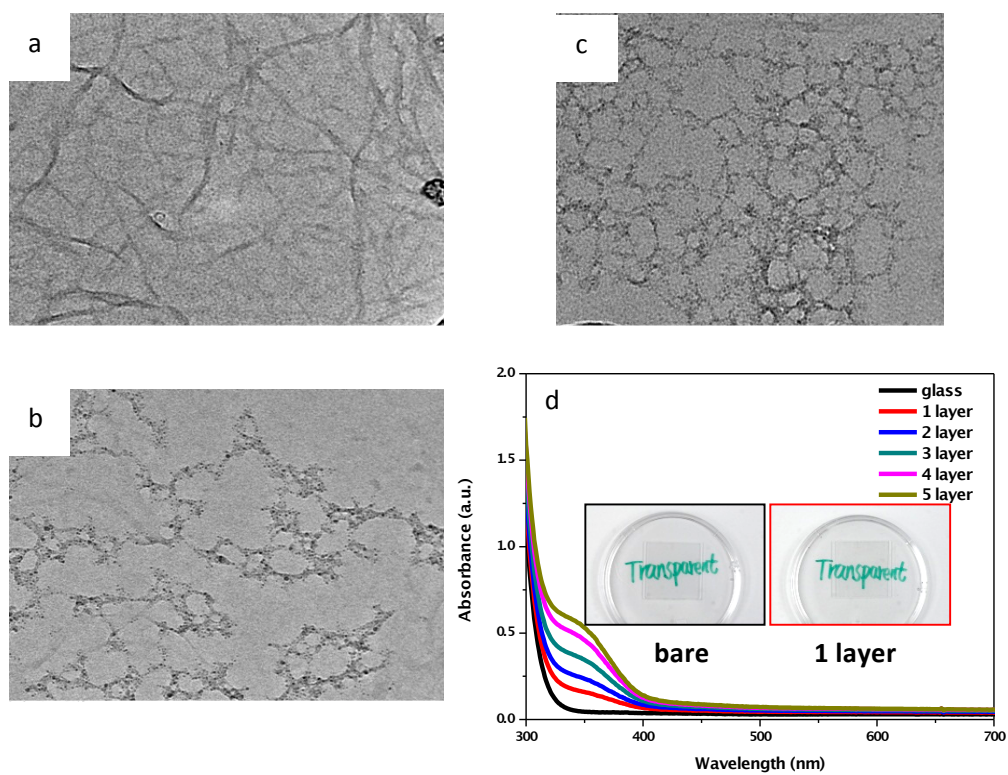


Figure 2. TEM images of ANFs in solutions of (a) DMSO, (b) PAA (1 %):DMSO=1:30 (v/v) and (c) PAA (1 %):DMSO=1:7.5 (v/v). (d) UV-Vis spectra of the glass slides before and after coating with different numbers of layers of the PAA/ANF suspension with the addition of 3 mL PAA. The insets show the optical images of the glass slides before and after coating one layer PAA/ANFs (thickness about 15 nm).

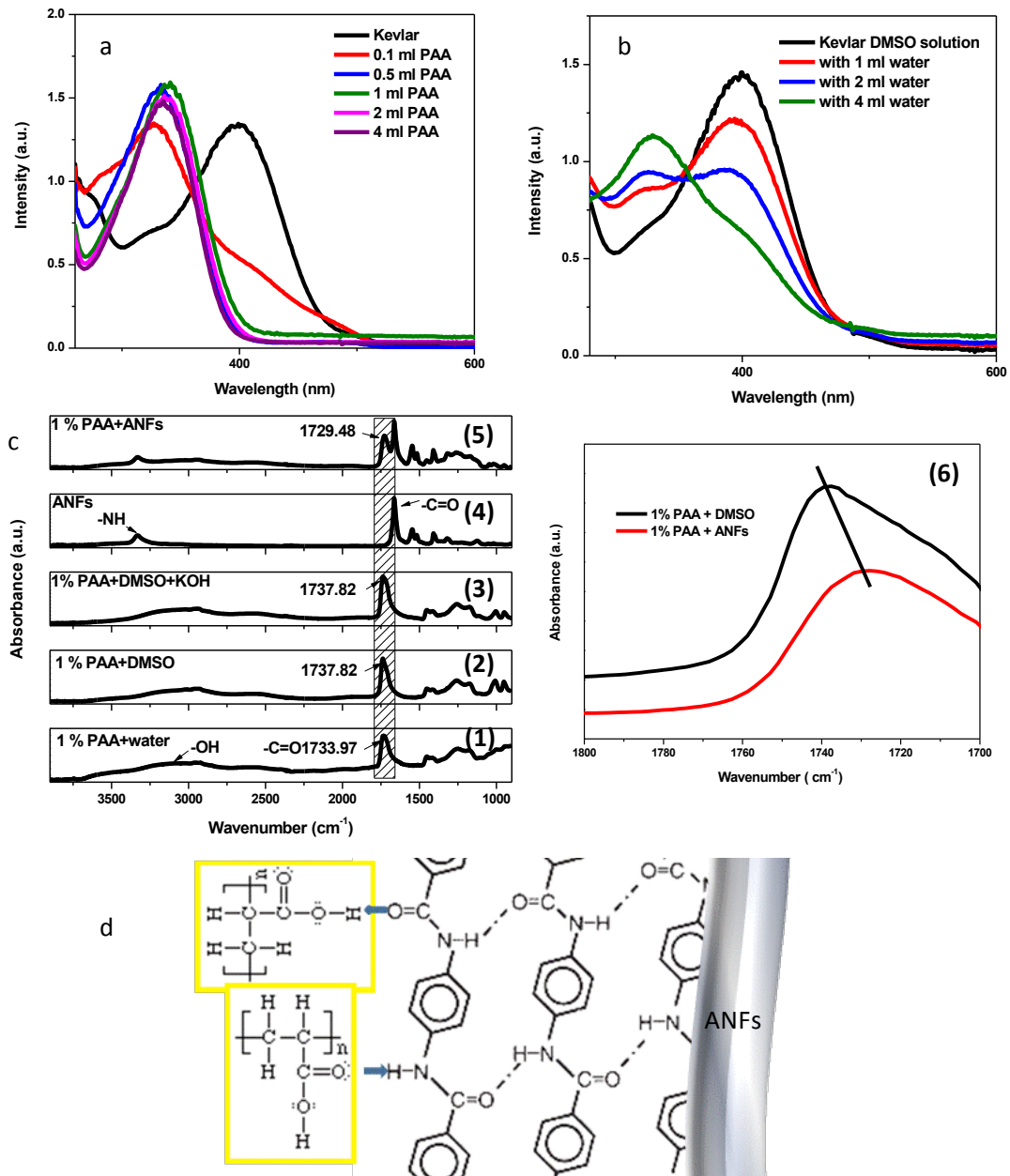


Figure 3. UV-Vis spectra showing the change of absorption upon the addition of different amounts of (a) PAA and (b) water. (c) IR spectra of (1-3) PAA in different solvent conditions, (4) ANFs, (5) a PAA/ANF mixture and (6) enlarged IR spectra showing the peak shift. (d) Schematic illustration of hydrogen bonding between PAA and ANFs.

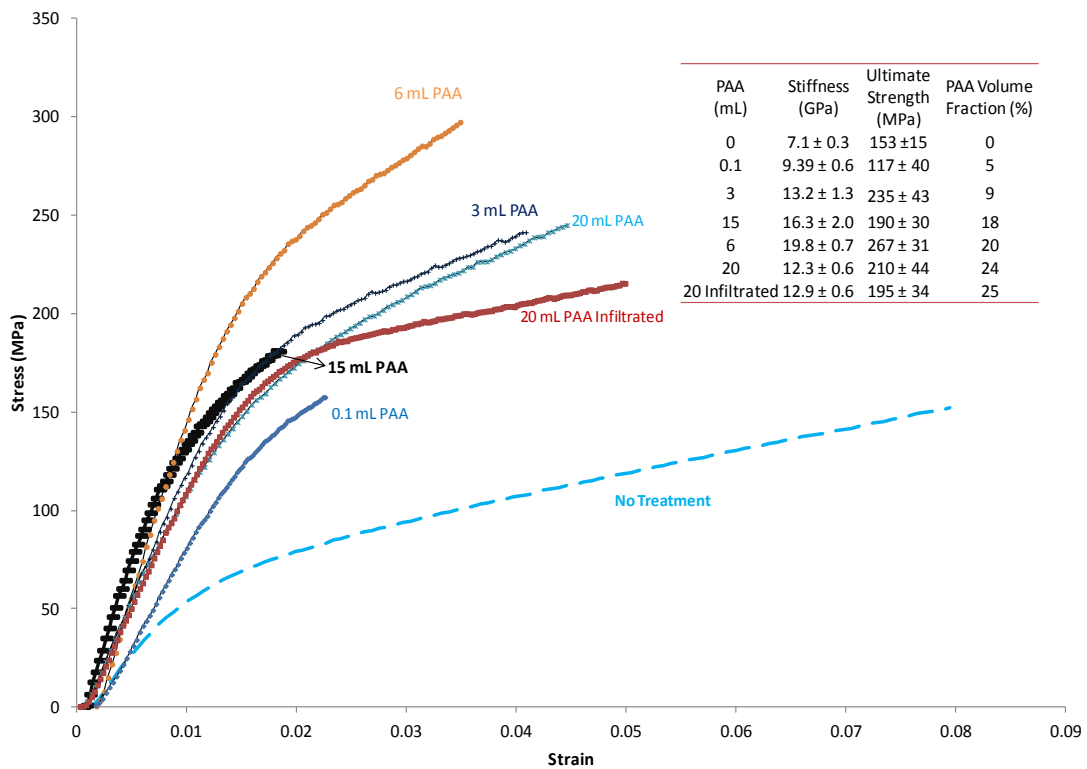


Figure 4. Stress-strain curves of PAA/ANF composite films with different volume fractions of PAA. Inset: summary of stiffness and ultimate strength of films with different PAA volume fractions.